Full Paper
doi.org/10.1002/chem.202000537

Thin Films

Comparative Solution Synthesis of Mn Doped (Na,K)NbO_3 Thin Films

Veronika Kovacova,*[a] Jung In Yang,[a] Leonard Jacques,[a] Song Won Ko,[b] Wanlin Zhu,[a] and Susan Trolier-McKinstry[a]

Abstract: $(K_{0.5}Na_{0.5})NbO_3$ (KNN) is a promising lead-free alternative for ferroelectric thin films such as $Pb(Zr,Ti)O_3$. One main drawback is its high leakage current density at high electric fields, which has been previously linked to alkali non-stoichiometry. This paper compares three acetate-based chemical solution synthesis and deposition methods for 0.5 mol% Mn-doped KNN film fabrication, using lower crystallization temperature processes in comparison to the sintering temperatures necessary for fabrication of KNN ceramics. This paper shows the crucial role of the A site homogenization step during solution synthesis in preserving alkali chemical homogeneity of Mn doped KNN films. Chemically homogeneous films show a uniform grain size of 80 nm and a leakage current density under 2.8×10^{-8} A cm^{-2} up to electric fields as high as 600 kV cm^{-1}, which is the highest breakdown strength reported for KNN thin films. Solution synthesis involving two-step pyrolysis resulted in films with dense, columnar microstructures, which are interesting for orientation control and enhancement of piezoelectric properties. This study reports detailed solution synthesis and deposition processes with good dielectric, ferroelectric and breakdown field properties. An optimized fabrication method that should couple low leakage current density with dense and oriented microstructures is proposed.

Introduction

Potassium sodium niobate (KNN) is an interesting alternative for lead-based ferroelectric thin films because it combines a high Curie temperature and good piezoelectric properties.[1,2] However, KNN is often reported to have higher leakage current densities[3] than films based on $PbZr_{1-x}Ti_xO_3$. One cause of the high field conductivity in KNN is the presence of secondary hygroscopic phases that result from non-stoichiometry, due to the alkali loss during the deposition process.[4] This issue can be at least partially resolved by optimizing deposition conditions, utilizing excess alkali, and doping.[3,5] High insulation resistance at high fields is essential in piezoelectric microelectromechanical systems (piezoMEMS) actuators in order to maximize displacement. Thus, there is an on-going need to further improve the insulation resistance in $K_{0.5}Na_{0.5}NbO_3$ films so that high fields can be used to offset the smaller $e_{31,f}$ piezoelectric coefficients relative to $PbZr_{0.52}Ti_{0.48}O_3$ piezoMEMS.

Several deposition methods have been explored to manufacture KNN: physical vapor deposition techniques such as sputtering,[6–8] pulsed laser deposition (PLD),[6,9] metalorganic chemical vapor deposition (MOCVD),[10] and chemical solution deposition (CSD).[11–19] The CSD method is cost effective, facile in the ability to rapidly change solution stoichiometry and doping, and is readily scalable to large or unusual (metal foil) substrates. Therefore, this paper discusses optimization of KNN deposition using the CSD method, with the intent of identifying factors that control the high field leakage current density.

Solution methods for KNN deposition are categorized according to the starting alkali precursors into acetate-based[11,13,14,18,20–23] and alkoxide-based[15,16,24–30] approaches. In both cases, niobium ethoxide is usually employed as the Nb precursor and 2-MOE (2-methoxyethanol) or 1,3-propanediol as solvents.[18,31] Acetate-based solutions have been shown to crystallize into single-phase perovskite KNN at lower temperatures than alkoxide-derived films.[12] This is useful as the thermal stresses in the piezoelectric film are reduced for lower crystallization temperatures. Therefore, the CSD methods discussed here are all acetate-based.

It has previously been reported that homogenization of the alkali concentration in the solution itself is critical to the preparation of high-quality KNN films. Several groups suggest that this is facilitated if the alkali precursors are dissolved and refluxed together in order to promote A site homogeneity prior to adding the Nb precursor. When this is not done, a longer reflux time is needed to reduce alkali segregation.[28,32] Howev-

[a] Dr. V. Kovacova, Dr. J. I. Yang, L. Jacques, Dr. W. Zhu, Prof. S. Trolier-McKinstry
Materials Science and Engineering Department and Materials Research Institute
The Pennsylvania State University
University Park, PA 16801 (USA)
E-mail: veronika@kovacova.fr

[b] Dr. S. W. Ko
Xaar, 316 Cambridge Science Park
Cambridge, CB4 OXR (UK)

Supporting information and the ORCID identification number(s) for the author(s) of this article can be found under: https://doi.org/10.1002/chem.202000537.

Part of a Special Issue on Low Temperature Solution Route Approaches to Oxide Functional Nanoscale Materials.

er, Chowdhury et al. reported that chemical segregation occurs in KNN gels even after long reflux times. As a result, alkali metal carbonates and bicarbonates developed after the pyrolyzed sample was exposed to air.[33]

A second approach to minimizing leakage current densities is to reduce alkali loss from the film on crystallization. Perovskite KNN is a stable phase.[4,7] However even a small non-stoichiometry[34] gives rise to alkali rich or deficient secondary phases such as K_3NbO_7, $K_4Nb_6O_{17}$, $K_2Nb_4O_{17}$, $K_6Nb_{44}O_{113}$,[35–37] and $K_{5.75}Nb_{10.85}O_{30}$, $K_3Nb_7O_{19}$, $K_2Nb_8O_{21}$, KNb_7O_{18} and $KNb_{13}O_{33}$ in ceramics and thin films.[38,39] $K_4Nb_6O_{17}$ easily forms stable hydrates, with water molecules intercalated in its layered structure.[40] Reported sodium niobate secondary phases are Na_3NbO_4, $NaNbO_3$, $Na_2Nb_8O_{21}$, $NaNb_7O_{18}$, and $NaNb_{10}O_{25}$.[41] These secondary phases could dramatically increase the leakage current of KNN.[42] To reduce this problem, solution stabilizers such as acetylacetone, acetic acid,[43] ethylenediaminetetraacetic acid (EDTA), monoethaloamine (MEA), diethanolamine (DEA),[29] and polyvinylpyrrolidone (PVP)[17,44] have been reported to increase deposition thickness per layer and to reduce alkali loss upon heating, improving leakage current density. Alternatively, in order to compensate alkali volatility, Na and K excess up to 20 mol% is utilized.[3,13,14]

A third approach to reducing leakage current is to dope the film to compensate for the as-produced carrier concentration. For example, it has been reported that manganese or lithium doping decreases leakage current densities in KNN films.[19,21,11,45] The fact that acceptor doping decreases the leakage current densities suggests that many KNN films are n-type as prepared.[46] This differs from most reports on KNN ceramics, which tend to be p-type.[47,48]

While some authors claim excellent environmental stability in their KNN films, Kupec et al., show that secondary phase can develop over time in some KNN films. Due to hydration and carbonization after 6 months of exposure to ambient air, some films become too conductive for characterization as dielectrics.[13]

Nonetheless, the functional properties of KNN films are interesting for piezoMEMS applications. The relative permittivity for undoped KNN films prepared by either acetate- and alkoxide-based routes was reported to range from 490 to 725 with dielectric loss ranging from 1.5 to 8% at 1 kHz.[13,14,16,20] Lee et al. reported relative permittivity values as high as 1050 for 0.5 mol% Mn-doped KNN films made by an acetate route. Additionally, it has been stated that relative permittivity increases with film thickness.[21] The remanent polarization in undoped KNN has been reported to range from 5 to 16.9 $\mu C\,cm^{-2}$ with coercive fields from 42 to 100 $kV\,cm^{-1}$.[3,13,15–17] Mn-doped KNN films have been reported to have remanent polarization from 7.5 to 15 $\mu C\,cm^{-2}$ with coercive fields from 36 to 100 $kV\,cm^{-1}$.[21,23,25] Wang et al. reported a piezoelectric coefficient $d_{33,f}$ as high as 78 $pm\,V^{-1}$ in an undoped, strongly {100}-oriented KNN film synthesized by an acetate route using PVP.[17] Some sol-gel processes result in very good piezoelectric film properties such as $e_{31,f} = -12\,C\,m^{-2}$ for 0.5 mol% Mn-doped KNN, though these results were given without many processing details.[19] As a result, it is not possible to directly reproduce the results. One of the lowest-reported leakage-current values for undoped KNN fabricated by sol-gel process is $1.8\times10^{-6}\,A\,cm^{-2}$ at 50 $kV\,cm^{-1}$.[49] Ahn et al. reached currents below $10^{-6}\,A\,cm^{-2}$ for fields under 80 $kV\,cm^{-1}$ for 20 mol% alkali excess.[3] More insulating properties are achieved with Mn, Li or Ta doping.[11,25,46,50–52] 0.5 mol% Mn-doped KNN films were reported to exhibit leakage current densities of around $3.6\times10^{-7}\,A\,cm^{-2}$ with breakdown fields of around 200 $kV\,cm^{-1}$[46] and $1\times10^{-7}\,A\,cm^{-2}$ at 100 $kV\,cm^{-1}$.[19] Matsuda et al. showed that a 1 mol% Mn-doped solid solution of 95 mol% $K_{0.5}Na_{0.5}NbO_3$ and 5 mol% $CaZrO_3$ exhibit leakage current densities of around $1\times10^{-7}\,A\,cm^{-2}$.[25]

What is then essential, for piezoMEMS actuators, is the development of environmentally stable, electrically insulating KNN films with high dielectric breakdown strengths. This paper compares three acetate-based solution-synthesis methods for 0.5 mol% Mn-doped KNN films fabrication and provides a detailed description of the synthesis processes. The microstructural quality, crystal orientation, dielectric, ferroelectric properties, breakdown strength and dielectric aging of films are given and correlated with different synthesis methods.

Experimental Section

0.5 mol% Mn-doped $K_{0.5}Na_{0.5}NbO_3$ (KNN) thin films were prepared by three chemical solution deposition (CSD) methods. In each case, 10 mol% K and 5 mol% Na excess was used to compensate for alkali volatilization, as K loss has been reported to be more severe than Na loss.[13,15] The precursors for the solutions include potassium acetate (CH_3COOK, 99%, Sigma Aldrich), sodium acetate (CH_3COONa, 99% Alfa Aesar), niobium pentaethoxide $(CH_3CH_2O)_5Nb$, 99.9%, Strem Chemicals Inc.) and manganese acetate ($(CH_3COO)_2Mn{\cdot}4H_2O$, 99.99%, Sigma Aldrich). 2-methoxyethanol ($CH_3OCH_2CH_2OH$, 99%, Sigma Aldrich), acetic acid (CH_3CO_2H, 99%, Sigma Aldrich) and acetic anhydride ($(CH_3CO)_2O$) were employed as solvents.

In this study, three alkali-based synthesis routes were investigated. In the first method, referred to as route A, alkali acetates were dissolved in acetic acid in a glove box. The solution was then refluxed at 105 °C for 10 min under an argon blanket for A site homogenization. A complete vacuum distillation of acetic acid from the mixture for 20 min followed. Nb ethoxide was combined with 2-MOE and stirred in the glove box separately at room temperature for 30 min. Nb ethoxide and 2-MOE solution was then combined with the precipitated alkali residue. Subsequently, a 4 h reflux under Ar at 105 °C helps improve mixing of the precursors at a molecular level and formation of oligomer cross-linking in the sol.[32] Finally, 0.1 mol of acetylacetone ($CH_3COCH_2COCH_3$, 99%, Sigma Aldrich) was added to the solution as a chelating agent, followed by 10 min stirring under Ar at room temperature. The final molarity of the solution was 0.4 M. The solution was aged in a refrigerator for one week, following recommendations in the literature.[53] This preparation method was inspired by work of Kupec et al. and Ahn et al.[3,13,20]

In the second method, referred to as route B, 50 mL 2-MOE and 5 mL of acetylacetone were combined at the beginning of the synthesis process and were homogenized by stirring at 80 °C for 20 min. Then, the Nb ethoxide precursor and the alkali acetate precursors were added one at a time to the solution and refluxed at 80 °C under Ar for 20 min. The mixture was refluxed in Ar for 4 h at

80 °C and then stirred under Ar for 24 h at room temperature. The molarity of the final solution was 0.4 M. One week of aging followed.[53] This method allows investigation of the effect of the alkali homogenization step replacement by a longer solution stirring.

In the third method, referred to as route C, alkali acetate precursors were combined with acetic anhydride within the glove box. The acetic anhydride reacts with water, producing acetic acid and therefore protects the precursors from being hydrated.[54,55] After refluxing at 105 °C for 10 min in Ar and complete vacuum distillation for 20 min, 20 mL of acetic anhydride was added into the alkali precipitate. Nb ethoxide and 30 mL 2-MOE were combined and stirred within the glove box, and then added to the alkali and acetic anhydride solution. The following steps were identical to the solution A route. Route C is similar to the Pechini method for solution preparation[31,56] since acetic anhydride combined with 2-MOE leads to the formation of esters at temperatures above 120 °C.[57] The principal interest of this method is to investigate the effect of acetic acid replacement for acetic anhydride as well as the effect of esterification. Figure 1 summarizes the three synthesis routes.

Powders were prepared for differential thermal analysis–thermogravimetric analysis (DTA-TGA) in order to determine an optimal pyrolysis conditions for films prepared from each solution. The solutions were dried in a glass container on a hotplate at 150 °C while stirring at 225 rpm to hasten evaporation. The dried powders were ground by hand with a metal spatula, then stored in a glass container and sealed with Parafilm®.

TGA was performed with a Discovery Series TGA Q600 by Texas Instruments. Approximately 10 mg of powder from each solution was placed in platinum crucibles. Powders were heated from room temperature to 800 °C at a rate of 10 °C min^{-1} under 100 mL min^{-1} of flowing air. The % weight loss as a function of temperature was recorded and is shown in Figure 2. All solutions show two mass drops, one centred at 280 ± 20 °C and a second centred at 560 ± 20 °C. Since 560 °C is above the crystallization temperatures for KNN secondary phase,[58] the pyrolysis temperature was set to 300 °C for all solutions. For the solution C process, a second step pyrolysis was added at 430 °C for 3 min to try to better eliminate organic compounds. A comparable 2 step pyrolysis was also utilized for some solution A films.

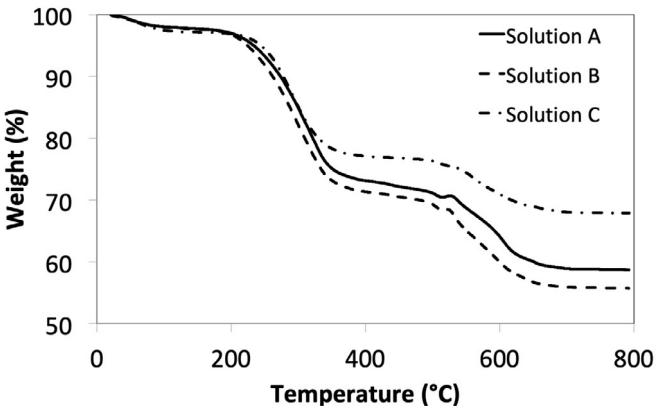

Figure 2. Thermo-gravimetric analysis profiles for solutions.

To deposit films, solutions were spun on platinized silicon wafers (Nova Electronics, Richardson, TX) at 3000 rpm for 30 s. Solution A and B layers were dried at 200 °C for 2 min and pyrolyzed at 300 °C for 3 min on hot plates. Solution C, and a subset of solution A layers underwent a second step pyrolysis at 430 °C for 5 min. All samples were crystallized at 750 °C for 5 min in air in a rapid thermal annealing (RTA) furnace. It is worth noting that temperatures involved in fabrication of KNN films by the sol-gel method are much smaller than that utilized for conventional sintering of KNN bulk ceramics.[59] The deposition process steps were repeated until the desired thickness was achieved. The final thickness of all films was 1 μm.

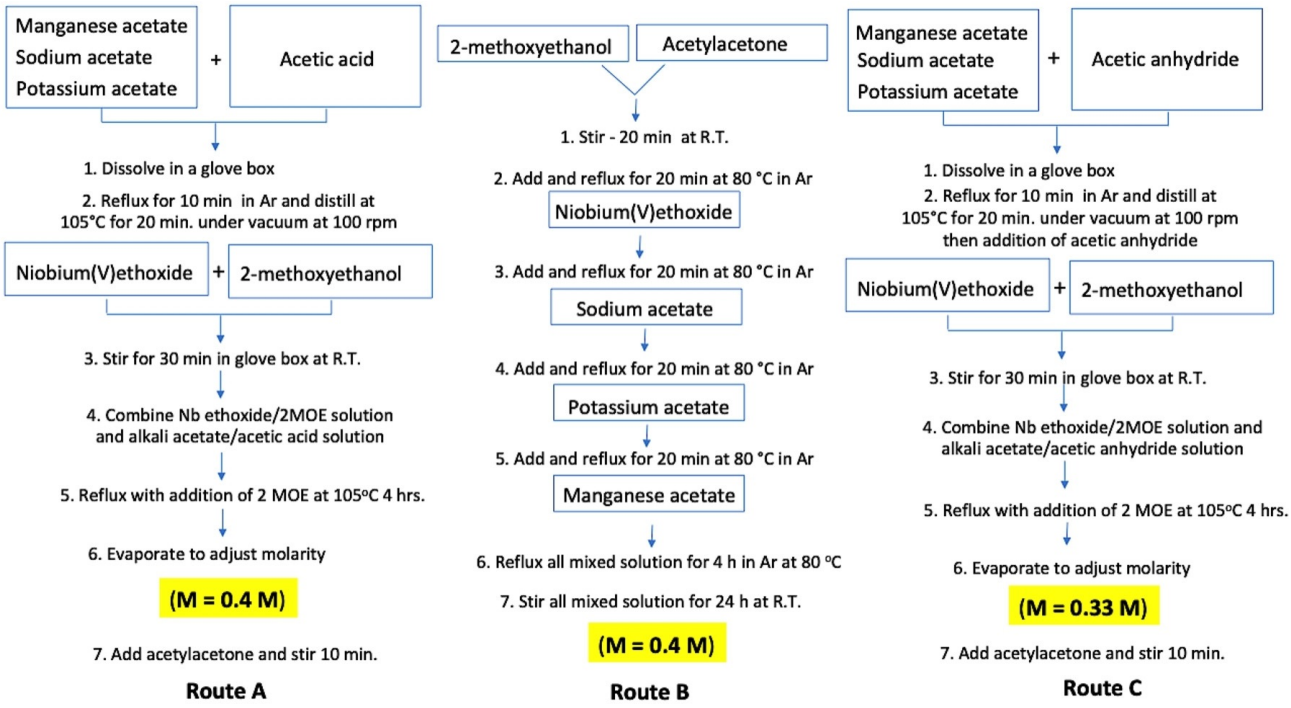

Figure 1. Solution synthesis process summary for route A, B and C.

High-resolution micrographs of the surface and cross-section of the KNN microstructure were obtained using field emission scanning electron microscopy (Zeiss Leo 1530 or Zeiss Merlin). A 5 kV accelerating voltage was used. Grain size was calculated by averaging seven measurements of the number of grains per linear distance across FESEM surface micrographs.

X-ray diffraction patterns for each film were collected with the Empyrean PANalytical laboratory diffractometer and Malvern Panalytical XPert Pro MPD in Bragg–Brentano geometry. The 2θ range was set from 10° to 70°. The degree of the {1 0 0} texture was estimated with the Lotgering factor,[60] calculated from integrated areas of pseudocubic peaks {1 0 0}, {1 1 0}, {2 1 0} and {2 1 1} from diffraction patterns using program PyMCA[61] and the Pseudo-Voigt function for profile fitting and PDF files 00-065-0276[62] corresponding to the tetragonal *P4mm* KNN phase. Note that diffraction peak {1 1 1} and {2 0 0} are omitted in the calculation because they are convoluted with {1 1 1} Pt peak and a substrate peak.

A Thermo Scientific Q250 SEM with an Energy Dispersive Spectroscopy (EDS) attachment was used to generate composition maps of the KNN films. An electron beam with 10 kV accelerating voltage and beam current of 100 nA were incident on the sample.

To pattern top electrodes for electrical measurements, a lift-off procedure was employed. LOR 5 and SPR 2013 positive photoresists were spun on to the sample surfaces and patterned by photolithography to create features with diameters of 200, 400, 500 or 600 μm. 100 nm thick Pt layer was deposited by RF sputtering (Kurt Lesker CMS-18 sputtering tool). After a standard lift-off process, Pt top electrodes were post-annealed in RTA at 500 °C, for 1 min in air to improve interface adhesion between the Pt electrodes and the KNN films.

Electrical measurements were made to assess the low and high field dielectric responses as well as the leakage currents of the films. The films' relative permittivity and dielectric loss were measured using an LCR meter (Hewlett Packard 4284A, Palo Alto, USA) from 50 Hz to 500 kHz with a 30 mV AC signal. A Multiferroic Test System (Radiant Technology, Inc. Albuquerque, NM) was used to perform high field polarization—electric field hysteresis loops (P-E loop) at 1 kHz and a maximum field of 400 kV cm^{-1}. The steady-state leakage current was evaluated as a function of the DC applied voltage by stepping up the voltage and waiting for a delay time (t_D) of 60 s prior to measuring the current with a Hewlett–Packard 4140 PA meter (Agilent Technology, Palo Alto, CA). Aging measurements were performed with 8 capacitors per DIP package for statistical data using a Hewlett–Packard 4284A precision LCR meter. Before the aging measurements were taken, the samples were poled at 150 kV cm^{-1} (two times the coercive field) for 10 minutes at 150 °C and cooled to room temperature while maintaining the dc voltage. Changes in the dielectric constant were monitored while probing samples at 10 kHz at 30 mV AC signal.[63]

Results and Discussion

Figure 3 displays the FESEM surface and cross-section images taken after deposition. Solution A films show a uniform 80 nm average grain size without a columnar microstructure and exhibit pores between grains. Solution B films show an average grain size of 230 nm with a nonuniform grain size distribution and porous microstructures. The cross-section for solution B films show larger grains but not a clear columnar microstructure. Solution C films show dense, columnar grain growth with

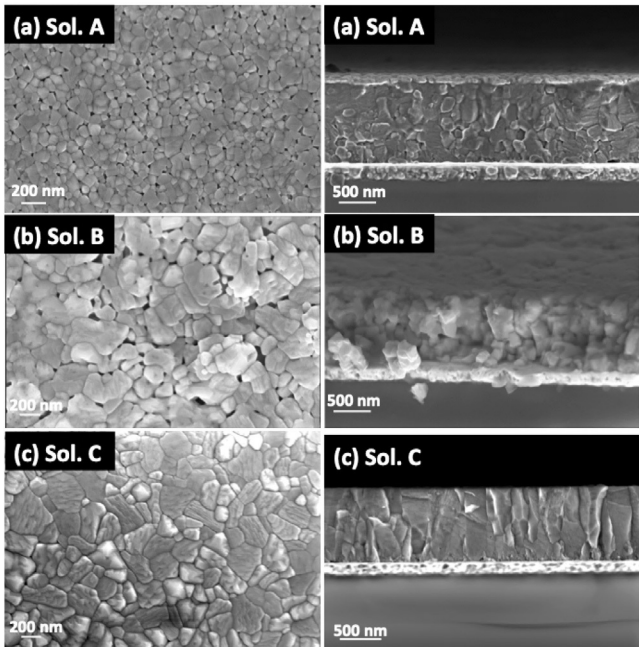

Figure 3. FESEM images showing surface and cross section for films prepared from solution A (a), B (b) and C (c) route.

an average grain size of 170 nm. However, the grain size distribution is not uniform.

The Nb and alkali chemical homogeneity of all films was investigated using EDS analysis. This technique has previously been used to quantify Na, K and Nb amounts in KNN films.[7] The qualitative results in Figure 4 show that solution A films are chemically homogeneous, but solution B and C films show Na and K rich regions. Since Nb concentration is homogeneous in all films, it is presumed that the effects of microstructural features on the EDS mapping are not dominant. It is worth noting that films with alkali chemical inhomogeneity also exhibit larger variations in grain size. Homogeneous grain size seems to be one of the signs of chemical homogeneity of films.

It is believed that the alkali segregation is directly traceable to the solution preparation procedure. The Solution A method includes an alkali homogenization step in acetic acid before addition of the niobium; this produces the most homogeneous alkali concentration in the resulting films. Solution B omits the alkali homogenization step. It is hypothesized that chemical inhomogeneity in the precursor solution produces the Na and K rich clusters in the dried gel and thus the chemical inhomogeneity in the films. Chowdhury et al. also combined all precursors without A-site homogenization, which led to Na and K segregation. Note that the segregation was diminished by a long reflux time up to 60 h.[28,33] The Solution C process replaces homogenization in acetic acid with homogenization in acetic anhydride. It must be noted that acetate alkali precursors do not dissolve in acetic anhydride; therefore, the homogenization of the perovskite A-site is not expected to be complete at this step. This is likely to be the reason for Na and K chemical segregation in the solution C films. To mitigate this, it

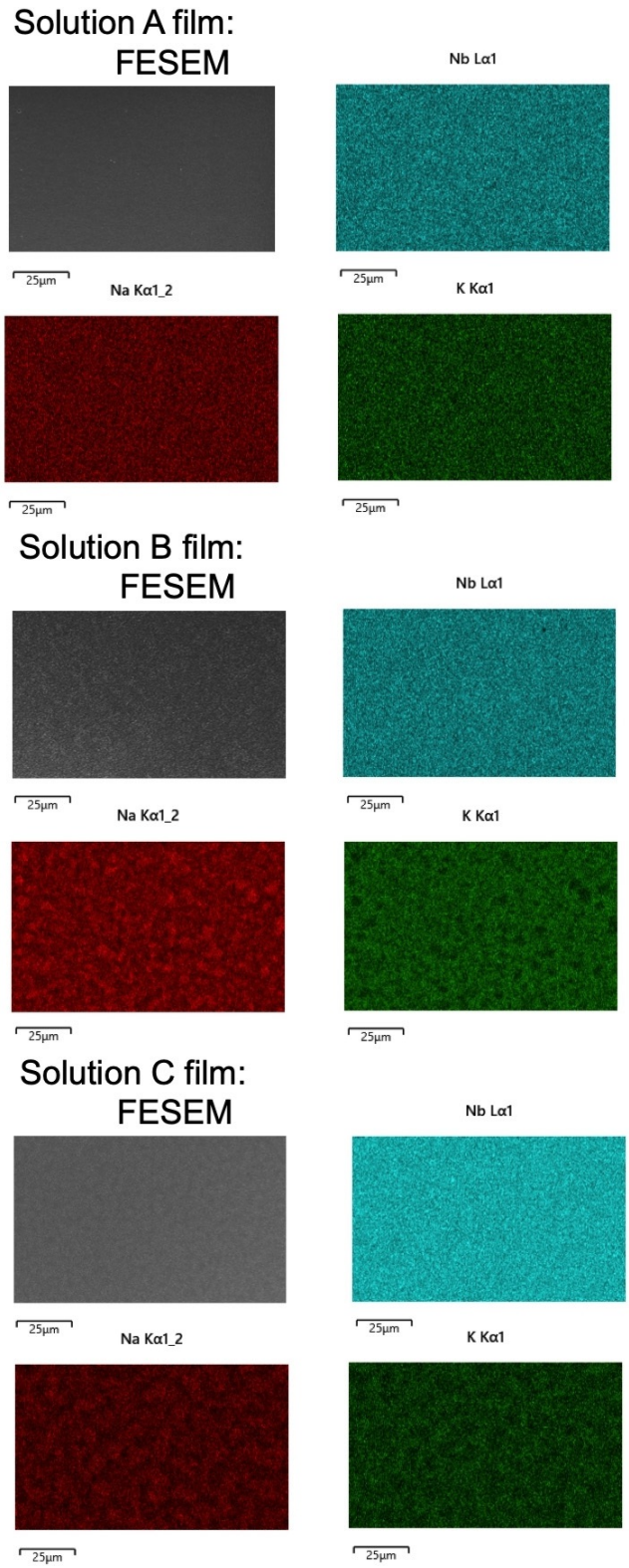

Figure 4. EDS analysis of film surface prepared from solution A, B and C routes.

is proposed that a combination of acetic acid with acetic anhydride should be used to reduce alkali segregation in KNN films.

Solutions A, B and C had different molarities and different deposition conditions. Solutions A and B had a molarity of 0.4 mol L^{-1} and the same deposition conditions, leading to a deposition thickness of 70 and 60 nm per layer, respectively. Solution C films had a molarity of 0.33 mol L^{-1} and two-step pyrolysis leading to a deposition thickness of 42 nm per layer. In order to achieve 1 μm thickness 15 layers need to be deposited from solution A, 17 layers need to be deposited from solution B and 24 layers need to be deposited from solution C.

Figure 5 shows the X-ray diffraction patterns of films from solutions A, B and C. All films crystallized in the perovskite phase. No secondary phase is observed. Diffraction peaks were indexed using the pseudocubic perovskite phase.

The Lotgering factor was used in order to compare the strength of the {100} texture in films. Table 1 shows the calculated Lotgering factors for {100} family of diffraction planes for the three films. All films have some degree of [100] orientation. Films from the solution C route are the most {100} textured. This observation correlates with the degree of columnar character in the microstructure. Columnar grains result from a preferential grain growth over nucleation during crystallization, and favour a preferential orientation of crystals. Films from solution C had the densest and the most homogeneous columnar grain microstructure, which results in the most {100} textured films.

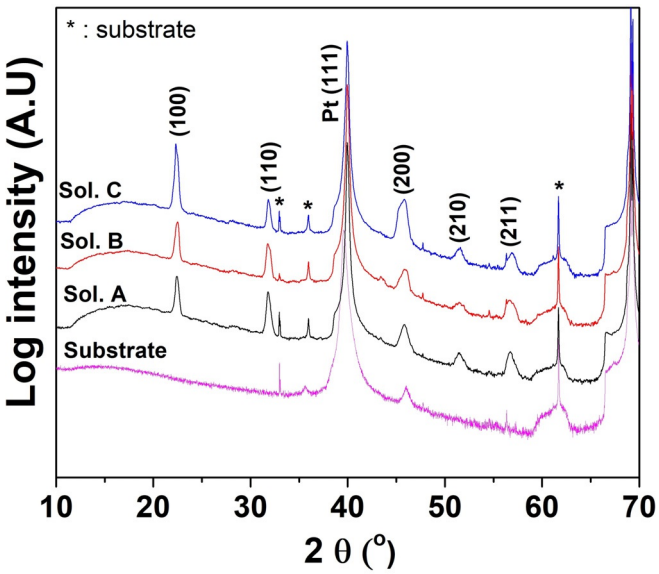

Figure 5. X-ray diffraction patterns for films from solution A, B, C routes and the substrate. Peaks at 2θ values of 33.02°, 36.00° and 61.75° correspond, respectively to the substrate, (111) Pt and (400) Si.

Table 1. Lotgering factor for {100} planes for films from solution A, B and C.

Film	Lotgering factor {100}
A	0.31
B	0.43
C	0.81

The second pyrolysis step used in solution C films leads to a denser microstructure with columnar grains (Figure S1 in Supporting Information). This change in microstructure due to pyrolysis could be due either to a change in the nucleation density or potentially to improved removal of organics. It is notable that when a 2-step pyrolysis was used for solution A, the density was also improved, as described below.

Films from solution C showed the highest relative permittivity of 970, in comparison to films from solution A and B, which are both 750 measured at 1 kHz as shown in Figure 6a; this permittivity is comparable to prior reports in the literature, and is consistent with the observation of residual porosity in both sets of films. Films A and C show low dielectric losses of around 1.6%; dielectric losses for solution B film are higher, 2.5%, at 1 kHz. Solution C films are close to the reported values for relative permittivity of dense Mn-doped KNN films.[21,46]

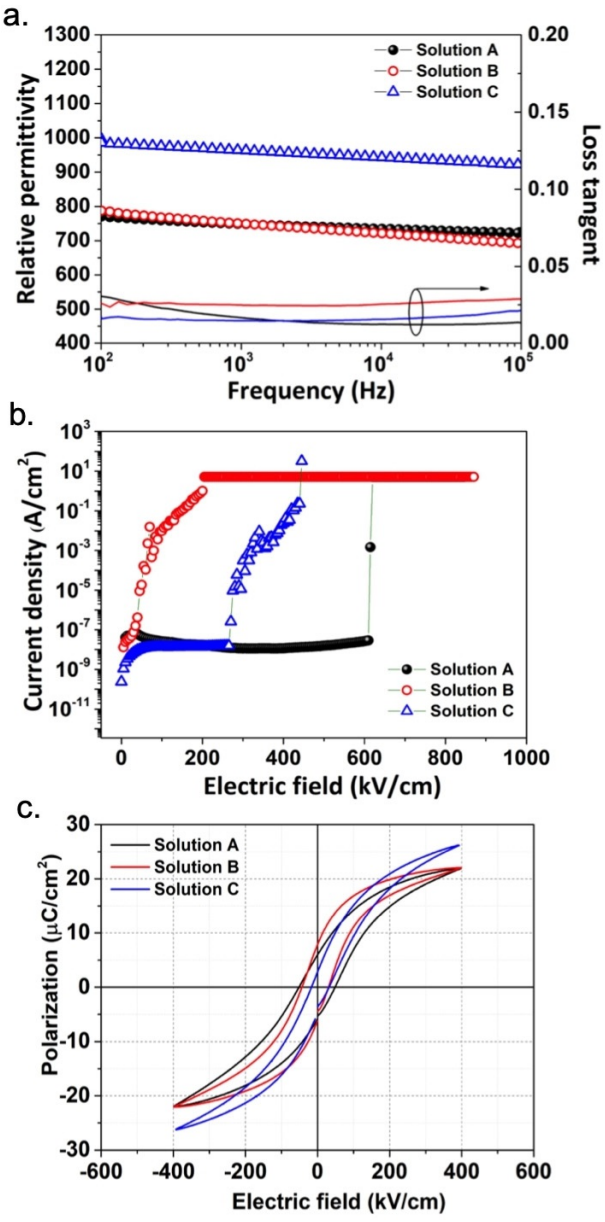

Figure 6. Relative permittivity and dielectric loss as a function of frequency (a), current density as a function of electric field (b) and polarization as a function of electric field (c) for films deposited from solution A (black), B (red) and C (blue) routes.

Current density measurements as a function of electric field are shown in Figure 6b. Solution B had the highest leakage current density; solution C films typically failed at 270 kV cm^{-1} whereas solution A films typically failed at 610 kV cm^{-1}. Moreover, the Solution A films conserved a low leakage current density of 2.8×10^{-8} A cm^{-2} up to electric field of 600 kV cm^{-1}, which is the highest electric field among the three solution preparation methods. It is also notable that the breakdown strengths of solution A films exceed prior reports for KNN films. For example, 0.5 mol% Mn doped KNN films were reported to exhibit leakage current densities of around 3.6×10^{-7} A cm^{-2} with breakdown fields of around 200 kV cm^{-1}.[46] It is worth noticing that solution A films exhibits low leakage current density up to large electric field despite the porous microstructure.

Figure 6c shows the polarization versus electric field data for films from solutions A, B and C. All films exhibit ferroelectricity. The coercive fields are 50, 36, and 25 kV cm^{-1} for films A, B and C respectively. The remanent polarization is 5.7, 6.6, and 4.0 μC cm^{-2} for films from solutions A, B, and C, respectively. Note that values of remanent polarization are lower than values reported previously for Mn-doped KNN films[21,23,25] on Si substrates; the reason for this discrepancy is not known. Films from solution A have a larger coercive field and slightly asymmetric P-E loop in comparison to solution C and B films. Films from solution B and C show an imprint off-centring their P-E loop by 6 to 8 kV cm^{-1}, respectively. This imprint might be related to existence of internal electric fields due to the chemical inhomogeneity of the films.

The aging rate of the dielectric constant for films from solution A, B and C routes were measured by monitoring the change in dielectric constants over time after the poling field was removed. Figure 7 shows that the aging rates of ε_r are 1.4%, 1.6% and 1.7% per decade for films from solutions A, B, and C, respectively. The decrease in the dielectric constant might be related to partial de-poling or reorientation of domains in KNN films over time. The slightly lower aging rate for the most chemically homogeneous film may be associated with reduced local fields in the sample, although in the future, this should be verified with denser films.

The correlation between low breakdown strength and large grains, as seen here in solution B and C films, has already been reported in the literature. Kupec et al. observed increased KNN grain size related to 10 mol% excess of Na or K in the films. The corresponding films also exhibited large leakage current densities. The grain boundaries of those samples were subsequently investigated with transmission electron microscopy and conductive atomic force microscopy.[13,14] Results show an amorphous material that wetted the grain boundaries, forming low resistance conduction paths through the film. The composition of this material is reported to be non-stoichiometric. Note that this material is not visible in X-ray diffraction patterns. On the other hand, Tanaka et al. observed that abnormal KNN grains are related to alkali ratio inhomogeneity.[16]

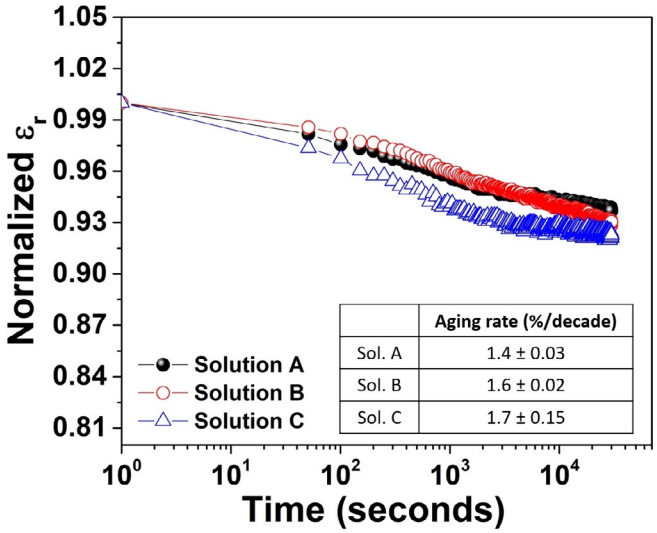

Figure 7. Aging of the dielectric constant (ε_r) for films from solution A (a), B (b) and C (c) routes. All samples were poled at two times the coercive field for 10 minutes at 150 °C. Changes in dielectric constant over time were monitored in order to determine the aging rate.

In order to assess whether low leakage current in case of solution A films is related to solution homogeneity or conductive grain boundaries, and in order to try to induce {1 0 0} texture in solution A films, an experiment using two-step pyrolysis on solution A, was performed (Figures S2 to S4 in the Supporting Information). 15 layers were deposited in order to achieve 1 μm film thickness. As expected, introduction of the second pyrolysis step at 430 °C, resulted in improvement in film density. An FESEM image of the film surface in Figure S2 c, shows fewer pores and a larger average grain size of 132 nm. The film cross-section image in Figure S2 d shows fewer pores and larger grains. Even though the microstructure in not columnar, the film cross-section contains fewer grains through the thickness. The grain size distribution is homogeneous, which was previously linked to alkali chemical homogeneity in the solution A films. It is noted that the modified deposition condition does not seem to affect alkali chemical homogeneity. Therefore, the hypothesis of alkali chemical homogeneity linked to solution synthesis process seems to be verified here. In addition, since second step pyrolysis resulted in denser microstructure and larger grains, it is possible that porous microstructure in films from solution A with one step pyrolysis were related to insufficient organics removal before crystallization.

Figure S3 compares the XRD patterns for films from solution A with one- or two-step pyrolysis. One can notice emergence of a peak at 28° in the pattern for solution A with two-step pyrolysis, which corresponds to the $K_4Nb_6O_{17}$ secondary phase, that is known for formation of hydrates.[40] The Lotgering factor for {1 0 0} orientation of the film from solution A with two-step pyrolysis is 0.27. This might be related to the lack of columnar microstructure. According to the TGA data, solution C experiences smaller weight loss in comparison to solutions A and B, which means that samples from solution A and B may need longer thermal treatments in order to burn organics. It is hypothesised that a columnar microstructure could be achieved in solution A with longer pyrolysis steps.

Electrical measurements shown in Figure S4 a show that the additional pyrolysis step results in a small increase of the relative permittivity from 750 to 780 measured at 1 kHz for the same film thickness, presumably due to a denser microstructure. The dielectric loss decreased slightly from 1.6% to 1% at 1 kHz for the same film thickness.

The leakage current measurements in Figure S4 b show that two-step pyrolysis on solution A decreases the film's breakdown voltage from 600 to 230 kV cm^{-1}. The two-step pyrolysis in solution A results in similar leakage current profile as for solution C films. Solution C and solution A films with two-step pyrolysis result in larger grain size. These results favour a hypothesis linking high leakage current to larger grain size forming more conductive pathways between the electrodes.[13] Considering the observation of secondary amorphous phase located at the KNN grain boundaries reported by Kupec et al.,[14] resulting in high leakage currents in KNN films, it is hypothesized that either optimization of the solution composition to avoid as much alkali excess or additional thermal treatment to crystallize the secondary amorphous phase might be efficacious.

Knowing that the secondary phase is located at the grain boundaries, one can consider the amount of secondary phase and the available surface area in each case. Films with smaller grains contain more grain boundary surface area thus the amount of secondary phase at the grain boundaries is diluted over more surface area. These grain boundaries might appear to be less conductive. The film with larger grains contains less available grain boundary surface area, thus similar or larger amount of secondary phase is more concentrated, which can result in more conductive grain boundaries. According to this hypothesis, a lower leakage current would be achievable with careful tuning of excess of alkali in KNN solutions.

All in all, this paper provides detailed process descriptions for KNN films fabrication using the CSD method, resulting in very good dielectric, ferroelectric and excellent insulating properties that are indispensable for piezoelectric MEMS actuators. The solution A synthesis route and associated deposition conditions led to chemically homogeneous films with high breakdown strength of about 600 kV cm^{-1} and low leakage current density of 2.8×10^{-8} A cm^{-2}. The downside of this method is a porous microstructure, lacking columnar grain growth and only a small degree of {1 0 0} orientation. The solution B synthesis route led to films with larger remanent polarization and larger Lotgering factor for {1 0 0} texture than the solution A process. However, this method also resulted in chemically heterogeneous films that had higher dielectric losses and lower breakdown strength than films A and C. The solution C synthesis route and deposition process gave rise to films with dense columnar microstructures. Films were {1 0 0} oriented with a Lotgering factor as high as 0.81. These films also exhibited high relative permittivity and low dielectric losses. On the other hand, solution C route resulted in chemically heterogeneous films, lower relative permittivity than reported 0.5 mol% Mn-doped KNN films and lower breakdown strength than solution A route films. Solution A with two-step pyrolysis resulted

in a denser microstructure linked to higher relative permittivity in comparison to films from solution A with one step pyrolysis. However, these films did not conserve high breakdown strength. The breakdown strength of solution A with two-step pyrolysis is of the similar magnitude as that of the solution C films. It is hypothesized that fine-tuning of alkali excess is required in order to achieve low leakage currents in KNN films with columnar grain microstructure.

Based on this work, process modifications are suggested in order to achieve better microstructural and electrical properties in KNN films. EDS images show that A-site homogenization step in either acetic acid or a mixture of acetic acid and acetic anhydride in needed in order to achieve KNN films with uniform alkali concentrations and uniform film surface topography. In order to favour {1 0 0} orientation in pore-free KNN films, columnar grain growth will be important. This in turn will favour piezoelectric coefficients; the two-step pyrolysis is preferred for this purpose. According to the literature, high leakage currents in films are related to the secondary amorphous phase located at the grain boundaries. Denser and columnar microstructure favours high concentration of secondary phase at the grain boundaries. Therefore, in order to reduce the leakage current, a fine-tuning of alkali excess in solutions will be necessary. Thus, it is suggested that in the future, adjusted alkali excess in the solution A preparation method with longer 2-step pyrolysis or fine-tuned alkali excess in solution C preparation method with an improved alkali homogenization step could be modified, such that high breakdown strength, high density, and high levels of orientation can be combined in a single KNN film.

Conclusions

This paper compares in detail three solution synthesis methods for KNN films. Solution A produced chemically homogeneous films with homogeneous grain size and with the lowest leakage current density at high fields reported for KNN thin films. Highly insulating KNN films are an important achievement for lead-free piezoelectric MEMS actuator applications. Solution B films exhibited Na and K rich regions, large average grain sizes and porous microstructures. These films have high leakage current density and low electric breakdown strength. This suggests that the alkali homogenization step during solution synthesis is crucial in order to achieve homogeneity in films. The solution C route utilized a two-step pyrolysis. This method led to a dense, columnar-grain microstructure with {1 0 0} preferred orientation. Since the chemically homogeneous solution A film with two step pyrolysis resulted in films with lower breakdown strength than films with one step pyrolysis, it seems that fine adjustments of alkali excess are necessary to achieve low leakage current density in KNN films with large-grain microstructure. Important conditions for KNN films fabrication include an A-site homogenization step, two-step pyrolysis and fine alkali tuning which enables pore free columnar grain microstructure with low leakage current densities in KNN films.

Acknowledgements

This material is based upon work supported in part by the National Science Foundation, as part of the Center for Dielectrics and Piezoelectrics under Grant Nos. IIP-1841453 and 1841466. The authors would like to acknowledge the National Science Foundation CPS grant (CNS 16-46399) for funding this research. The authors are thankful to Gino Tambourine from the Materials Characterization Laboratory at the Pennsylvania State University for his help with the thermo-gravimetric analysis.

Conflict of interest

The authors declare no conflict of interest.

Keywords: alkali chemical homogeneity · lead-free ferroelectric films · leakage current density · sodium potassium niobate · sol–gel CSD

[1] T. R. Shrout, S. Zhang, *J. Electroceram.* **2007**, *19*, 185.
[2] B. Jaffe, W. R. Cook Jr., H. Jaffe, *Piezoelectric Ceramics*, Academic Press, London and New York, **1971**.
[3] C. W. Ahn, S. Y. Lee, H. J. Lee, A. Ullah, J. S. Bae, E. D. Jeong, J. S. Choi, B. H. Park, I. W. Kim, *J. Phys. D* **2009**, *42*, 215304.
[4] A. Safari, E. K Akdogan, *Piezoelectric and Acoustic materials for Transducer Application*, Springer US, **2008**.
[5] H. J. Seog, A. Ullah, C. W. Ahn, *J. Korean Phys. Soc.* **2018**, *72*, 1467 – 1483.
[6] S. Khartsev, A. Grishin, J. Andreasson, J. H. Koh, J. Song, *Integr Ferroelectr.* **2003**, *55*, 769 – 779.
[7] K. Shibata, F. Oka, A. Ohishi, T. Mishima, I. Kanno, *Appl. Phys. Express* **2008**, *1*, 011501.
[8] Z. G. Zhang, S. I. Khartsev, A. M. Grishin, *Integr Ferroelectr.* **2004**, *67*, 59 – 68.
[9] C. R. Cho, A. Grishin, *J. Appl. Phys.* **2000**, *87*, 4439 – 4448.
[10] C. R. Cho, B. M. Moon, *Integr Ferroelectr.* **2002**, *45*, 39 – 48.
[11] C. W. Ahn, E. D. Jeong, S. Y. Lee, H. J. Lee, S. H. Kang, I. W. Kim, *Appl. Phys. Lett.* **2008**, *93*, 212905.
[12] L. Čakare-Samardžija, B. Malič, M. Kosec, *Ferroelectrics* **2008**, *370*, 113 – 118.
[13] A. Kupec, B. Malič, J. Tellier, E. Tchernychova, S. Glinšek, M. Kosec, *J. Am. Ceram. Soc.* **2012**, *95*, 515 – 523.
[14] A. Kupec, H. Uršič, R. C. Frunză, E. Tchernychova, B. Malič, *J. Eur. Ceram. Soc.* **2015**, *35*, 3507 – 3511.
[15] Y. Nakashima, W. Sakamoto, T. Shimura, T. Yogo, *Jpn. J. Appl. Phys.* **2007**, *46*, 6971 – 6975.
[16] K. Tanaka, H. Hayashi, K. I. Kakimoto, H. Ohsato, T. Iijima, *Jpn. J. Appl. Phys.* **2007**, *46*, 6964 – 6970.
[17] L. Wang, K. Yao, P. C. Goh, W. Ren, *J. Mater. Res.* **2009**, *24*, 3516 – 3522.
[18] S. Wiegand, S. Flege, O. Baake, W. Ensinger, *J. Alloys Compd.* **2013**, *548*, 38 – 45.
[19] S. S. Won, J. Lee, V. Venugopal, D. J. Kim, J. Lee, I. W. Kim, A. I. Kingon, S.-H. Kim, *Appl. Phys. Lett.* **2016**, *108*, 232908.
[20] B. Malič, A. Kupec, K. Vojisavljević, T. Pečnik in *Lead-Free Ferroelectric Thin Films, in Handbook of Sol-Gel Science and Technology* (Eds.: L. Klein, M. Aparicio, A. Jitianu), Springer, Cham, Switzerland **2016**.
[21] S. Y. Lee, H. J. Seog, C. W. Ahn, A. Ullah, I. W. Kim, *Jpn. J. Appl. Phys.* **2012**, *51*, 09MD03.
[22] M. A. M. Hatta, M. W. A. Rashid, U. A. A. H. Azlan, N. A. Azmi, M. A. Azam, T. Moriga, *Mater. Res.* **2016**, *19*, 1417 – 1422.
[23] L. Wang, W. Ren, P. C. Goh, K. Yao, P. Shi, X. Wu, X. Yao, *Thin solid films* **2013**, *537*, 65 – 69.
[24] C. C. Lin, C. W. Su, *Appl. Surf. Sci.* **2018**, *428*, 199 – 206.
[25] T. Matsuda, W. Sakamoto, B.-Y. Lee, T. Iijima, J. Kumagai, M. Moriya, T. Yogo, *Jpn. J. Appl. Phys.* **2012**, *51*, 9S1.

[26] C. Kang, C. Kan, J.-H. Park, D. Shen, H. Ahn, M. Park, D.-J. Kim, *J. Sol-Gel Sci. Technol.* **2011**, *58*, 85 – 90.
[27] S. W. Zhang, J. Luo, Z. Zhou, J. F. Li, *J. Am. Ceram. Soc.* **2019**, *102*, 2696 – 2705.
[28] A. Chowdhury, J. Bould, M. Londesborough, E. Večerníková, S. J. Milne, *Mater. Chem. Phys.* **2010**, *124*, 159 – 162.
[29] P. C. Goh, K. Yao, Z. Chen, *Appl. Phys. Lett.* **2011**, *99*, 092902.
[30] Q. Yu, J. F. li, Y. Chen, L. Q. Cheng, W. Sun, Z. Zhuo, Z. Wang, *J. Am. Ceram. Soc.* **2014**, *97*, 107 – 113.
[31] T. Schneller, R. Waser, M. Kosec, D. Payne, *Chemical Solution Deposition of Functional Oxide Thin Films*, Springer Verlag Gmbh, **2013**.
[32] A. Chowdhury, J. Bould, M. G. S. Londesborough, S. J. Milne, *J. Solid State Chem.* **2011**, *184*, 317 – 324.
[33] A. Chowdhury, J. Bould, M. G. S. Londesborough, S. J. Milne, *Chem. Mater.* **2010**, *22*, 3862 – 3874.
[34] A. Popovič, L. Bencze, J. Koruza, B. Malic, *RSC Adv.* **2015**, *5*, 76249 – 76256.
[35] A. Reisman, F. Holtzberg, *J. Am. Ceram. Soc.* **1955**, *77*, 2115 – 2118.
[36] N. Helth Gaukås, S. M. Dale, T. M. Ræder, A. Toresen, R. Holmestad, J. Glaum, M.-A. Einarsrud, T. Grande, *Materials* **2019**, *12*, 2042.
[37] X. Vendrell, O. Raymond, D. A. Ochoa, J. E. Gracía, L. Mestres, *Thin solid films* **2015**, *577*, 35 – 41.
[38] R. S. Roth, *Prog. Solid. St. Chem.* **1980**, *13*, 159 – 192.
[39] E. Irle, R. Blachnik, B. Gather, *Thermochim. Acta* **1991**, *179*, 157 – 169.
[40] M. A. Bizeto, V. R. L. Constantino, *Mater. Res. Bull.* **2004**, *39*, 1729 – 1736.
[41] M. W. Shafer, R. Roy, *J. Am. Ceram. Soc.* **1959**, *42*, 482 – 486.
[42] B. Malič, J. Koruza, J. Hreščak, J. Bernard, K. Wang, J. Fisher, A. Benčan, *Materials* **2015**, *8*, 5449.
[43] X. Yan, W. Ren, X. Wu, P. Shi, X. Yao, *J. Alloys Compd.* **2010**, *508*, 129 – 132.
[44] Y. Wang, K. Yao, M. S. Mirshekarloo, F. E. H. Tay, *J. Am. Ceram. Soc.* **2016**, *99*, 1631 – 1636.
[45] F. Lai, J. F. Li, Z.-X. Zhu, Y. Xu, *J. Appl. Phys.* **2009**, *106*, 064101.
[46] S. Y. Lee, C. W. Ahn, A. Ullah, H. J. Seog, J. S. Kim, S. H. Bae, I. W. Kim, *Curr. Appl. Phys.* **2011**, *11*, S266 – S269.
[47] L. Liu, Y. Huang, C. Su, L. Fang, M. Wu, C. Hu, H. Fan, *J. Appl. Phys. A* **2011**, *104*, 1047 – 1051.
[48] S. Wu, W. Zhu, L. Liu, D. Shi, S. Zheng, Y. Huang, L. Fang, *J. Electron. Mater.* **2014**, *43*, 1055 – 1061.
[49] G. Li, X.-Q. Wu, W. Ren, P. Shi, X.-F. Chen, X. Yao, *Ceram. Intern.* **2012**, *38 – 31*, S279 – 281.
[50] C.-C. Lin, C.-C. Chen, C.-M. Weng, S.-Y. Chu, C.-S. Hong, C.-C. Tsai, *J. Appl. Phys.* **2015**, *117 – 118*, 085307.
[51] S. Y. Lee, C. W. Ahn, J. S. Kim, A. Ullah, H. J. Lee, H.-I. Hwang, J. S. Choi, B. H. Park, I. W. Kim, *J. Alloys Compd.* **2011**, *509*, L194 – L198.
[52] J. S. Kim, C. W. Ahn, A. Ullah, S. A. Chae, I. W. Kim, *J. Korean Phys. Soc.* **2016**, *68*, 1461 – 1466.
[53] Y. Xu, D. Liu, F. Lai, Y. Zhen, J. F. Li, *J. Am. Ceram. Soc.* **2008**, *91*, 2844 – 2847.
[54] "Sodium Acetate." Chemical Compounds, can be found under Encyclopedia.com: https://www.encyclopedia.com/science/academic-and-educational-journals/sodium-acetate, **2020**.
[55] 7.10—Sol-Gel Processing of Metal Compounds U. Schubert in *Comprehensive Coordination Chemistry II* (Eds.: J .A. McCleverty, T. J. Meyer), Pergamon, **2003**, pp. 629 – 656.
[56] A. Chowdhury, S. O'Callaghan, T. A. Skidmore, C. James, S. J. Milne, *J. Am. Ceram. Soc.* **2009**, *92*, 758 – 761.
[57] Y. Wang, W. Li, *React. Kinet. Catal. Lett.* **2000**, *69*, 169 – 176.
[58] I. Bretos, R. jimenes, J. Ricote, M. L. Calzada, *Chem. Soc. Rev.* **2018**, *47*, 291 – 308.
[59] J. F. Li, Y. Zhen, B. P. Zhang, L. M. Zhang, K. Wang, *Ceram. Intern.* **2008**, *34*, 783 – 786.
[60] F. K. Lotgering, *J. Inorg. Nucl. Chem.* **1959**, *9*, 113 – 123.
[61] V. A. Solé, E. Papillon, M. Cotte, Ph. Walter, J. Susini, *Spectrochim. Acta Part B* **2007**, *62*, 63 – 68.
[62] H. Mgbemere, M. Hinterstein, G. Schneider, *J. Eur. Ceram. Soc.* **2012**, *32*, 4341 – 4352.
[63] R. G. Polcawich, S. Trolier-McKinstry, *J. Mater. Res.* **2000**, *15*, 2505.

Manuscript received: January 31, 2020
Accepted manuscript online: April 9, 2020
Version of record online: June 12, 2020